

Proposed silicon wire interleaver structure

Junfeng Song,^{1,2,*} Q. Fang,¹ S. H. Tao,¹ M. B. Yu,¹ G. Q. Lo,¹ and D. L. Kwong¹

¹Institute of Microelectronics, A*STAR, 11 Science Park Road, Science Park II, Singapore 117685

²State Key Laboratory on Integrated Opto-electronics, College of Electronic Science and Engineering, Jilin University, 119 Jiefang Road, Changchun 130023, China

*songjf@ime.a-star.edu.sg

<http://ime.a-star.edu.sg/>

Abstract: A Ring-resonator Mach-Zehnder interferometer (RR-MZI) optical interleaver structure comprising a ring resonator (RR) and a 3 dB directional coupler is proposed. The interleaver is fabricated with 300 nm × 300 nm silicon wires on silicon-on-insulator (SOI) wafers. The fabricated interleaver demonstrates a flat-top spectral response, and the measured free spectral range (FSR) is ~20 nm. The insertion loss (IL) of the device is ~-10 dB and the polarization dependent loss (PDL) <5 dB. Both the experimental and simulation results are in good agreement.

©2008 Optical Society of America

OCIS Codes: (130.3120) Integrated optics devices; (130.2790) Guided waves; (220.0220) Optical design and fabrication; (220.4000) Microstructure fabrication; (230.0230) Optical devices; (230.3990) Microstructure devices.

References and links

1. S. Cao, J. Chen, J. N. Damask, C. R. Doerr, L. Guiziou, G. Harvey, Y. Hibino, H. Li, S. Suzuki, K. Y. Wu, and P. Xie, "Interleaver technology: comparisons and applications requirements," OFC' 03 Interleaver Workshop, pp. 1–9, <http://www.neophotonics.com/down/2.pdf>.
2. H. Arai, H. Nonen, K. Ohira, and T. Chiba, "PLC wavelength splitter for dense WDM transmission system," Hitachi Cable Review **21**, 11–16 (2002), http://www.hitachi-cable.co.jp/ICSFiles/afieldfile/2005/11/29/2_review03.pdf.
3. S. G. Heris, A. Zarifkar, K. Abedi, and M. K. M. Farshi, "Interleavers/deinterleavers based on Michelson-Gires-Tournois interferometers with different structures," in Proceedings of Semiconductor Electronics, Kuala Lumpur, Malaysia (ICSE 2004) **7–9**, pp. 573–576 (2004).
4. C. K. Madsen and J. H. Zhao, *Optical Filter Design and Analysis – A Signal Processing Approach* (Wiley, New York, 1999).
5. B. B. Dingel and M. Izutsu, "Multifunction optical filter with a Michelson–Gires–Tournois interferometer for wavelength-division-multiplexed network system application," Opt. Lett. **23**, 1099–1101 (1998).
6. C. H. Hsieh, R. B. Wang, Z. Q. James Wen, I. McMichael, P. C. Yeh, C. -W. Lee, and W. H. Cheng, "Flat-top interleavers using two Gires–Tournois etalons as phase-dispersive mirrors in a Michelson interferometer," IEEE Photon. Technol. Lett. **15**, 242–244 (2003).
7. J. Zhang, L. R. Liu, and Y. Zhou, "Novel and simple approach for designing lattice form interleaver filter," Opt. Express **11**, 2217–2224 (2003)..
8. C.-W. Lee, R. B. Wang, P. C. Yeh, and W.-H. Cheng, "Sagnac interferometer based flat-top birefringent interleaver," Opt. Express **14**, 4636–4643 (2006..
9. Y. Zhang, Q. J. Wang, and T. C. Soh, "Optical interleaver," US Patent #2005/0271323A1.
10. Q. J. Wang, Y. Zhang, and Y. C. Soh, "Efficient structure for optical interleavers using superimposed chirped fiber Bragg gratings," IEEE Photon. Technol. Lett. **17**, 387–389 (2005).
11. Q. J. Wang, Y. Zhang, and Y. C. Soh, "All-fiber 3 × 3 interleaver design with flat-top passband," IEEE Photon. Technol. Lett. **16**, 168–170 (2004).
12. K. Jinguji and M. Kawachi, "Synthesis of coherent two-port lattice-form optical delay-line circuit," J. Lightwave Technol. **13**, pp. 73–82 (1995).
13. K. Jinguji, "Synthesis of coherent two-port optical delay-line circuit with ring waveguides," J. Lightwave Technol. **14**, 1882–1884 (1996).
14. M. Oguma, T. Kitoh, K. Jinguji, T. Shibata, A. Himeno, and Y. Hibino, "Passband-width broadening design for WDM filter with lattice-form interleave filter and arrayed-waveguide gratings," IEEE Photon. Technol. Lett. **14**, 328–330 (2002).
15. S. Bidnyk, A. Balakrishnan, A. Del age, M. Gao, P. A. Krug, P. Muthukumar, and M. Pearson, "Novel architecture for design of planar lightwave interleavers," J. Lightwave Technol. **23**, 1435–1440 (2005).
16. C. G. H. Roeloffzen, R. M. de Ridder, G. Sengo, K. W orhoff, and A. Driessen "Passband flattened

interleaver using a Mach-Zehnder interferometer with ring resonator fabricated in SiON waveguide technology,” in Proceedings Symposium of IEEE/LEOS (IEEE, 2002) pp.32-35, <http://leosbenelux.org/symp02/s02p10.pdf>.

17. K. Wörhoff, C. G. H. Roeloffzen, R. M. de Ridder, G. Sengo, L. T. H. Hilderink, P. V. Lambeck, and A. Driessen, “Tolerance and application of polarization independent waveguide for communication devices,” in Proceedings Symposium of IEEE/LEOS (IEEE, 2004) pp. 107–110, <http://leosbenelux.org/symp04/s04p107.pdf>.
18. Z. P. Wang, S. J. Chang, C. Y. Ni, and Y. J. Chen “A high-performance ultracompact optical interleaver based on double-ring assisted Mach–Zehnder interferometer,” IEEE Photon. Technol. Lett. **19**, 1072–1074 (2007).
19. K. K. Lee, D. R. Lim, L. C. Kimerling, J. Shin, and F. Cerrina, “Fabrication of ultralow-loss Si/SiO₂ waveguides by roughness reduction,” Opt. Lett. **26**, 1888–1890 (2001).
20. H. Yamda, T. Chu, S. Ishida, and Y. Arakawa, “Optical directional coupler based on Si-wire waveguides,” IEEE Photon. Technol. Lett. **17**, 585–587 (2005).
21. H. Yamda, T. Chu, S. Ishida, and Y. Arakawa, “Si Photonic wire waveguide devices,” J. Lightwave Technol. **12**, 1371–1379 (2006).
22. D. Lauvernier, S. Garidel, M. Zegaoui, J. P. Vilcot, J. Harari, V. Magnin, and D. Decoster, “Optical devices for ultra-compact photonic integrated circuits based on III-V/polymer nanowires,” Opt. Express **15**, 5333–5341 (2006).

1. Introduction

Dense wavelength-division multiplexing (DWDM) is one of the key technologies for increasing the data transmission rate in optical fiber communications [1-3]. However, the DWDM system requires narrow channel spacing. As optical interleavers/deinterleavers are characterized by narrow channel spacing, they are ideal candidates for DWDM applications. Many optical filters have been investigated [4]. Interleavers were designed and implemented in many varieties, such as the Michelson–Gires–Tournois interferometer (MGTI) [5, 6], bulk birefringent crystals [7, 8], fibers [9-11], and the planar-light-wave circuit (PLC) [12-18]. Among them, the MGTI, the bulk birefringent crystals, and the fibers cannot be integrated with other devices on a chip. On the contrary, since the PLC is compatible with standard complementary metal-oxide-semiconductor technology, is compact, and is cost-effective, it is an attractive choice for DWDM applications.

Typically an interleaver requires a flat-top and near box-shaped spectral response. Jinguji *et al.* [12, 13] proposed a cascade structure to realize an arbitrary filtering response. However, owing to multiple stages used in the structure, the design and fabrication are complicated. Using only two stages in the lattices, Oguma *et al.* realized 50-GHz spacing on a 102-channel WDM filter with an insertion loss of 4 dB and a 1 dB bandwidth of 30 GHz [14]. Bidnyk *et al.* [15] reported a design of a DWDM interleaver based on planar echelle gratings, but it is difficult to deliver a top-flat response with such gratings. Roeloffzen *et al.* [16, 17] reported an interleaver with an approximately rectangular spectral response. The interleaver was comprised of an asymmetric Mach-Zehnder interferometer (MZI) in which a ring resonator was coupled to one of the branches of the MZI. Similarly, Wang *et al.* [18] presented an ultracompact optical interleaver based on a two-micro-ring-assisted Mach–Zehnder interferometer on a silica platform. Although the device exhibited a flat and nearly square passband, a $\pi/2$ phase difference between the two arms had to be introduced externally, and the circumference of the micro-rings had to be controlled exactly at two times the length of the delay line. In fact, an MZI structure with one delay line can fully function as an interleaver, and a ring can be employed to flatten the top of the passband spectrum.

In this paper we propose a ring-resonator Mach-Zehnder interferometer (RR-MZI) interleaver structure, which is comprised of a ring and a 3 dB directional coupler (DC) only. As the ring serves as both a splitter and a delay line, the proposed interleaver is more compact and easier to design. We will explain the principle of the interleaver and then optimize the structure. A device fabricated on silicon wires will be demonstrated and characterized, and discussions on the experimental results also will be presented.

2. RR-MZI structure

2.1 Principle

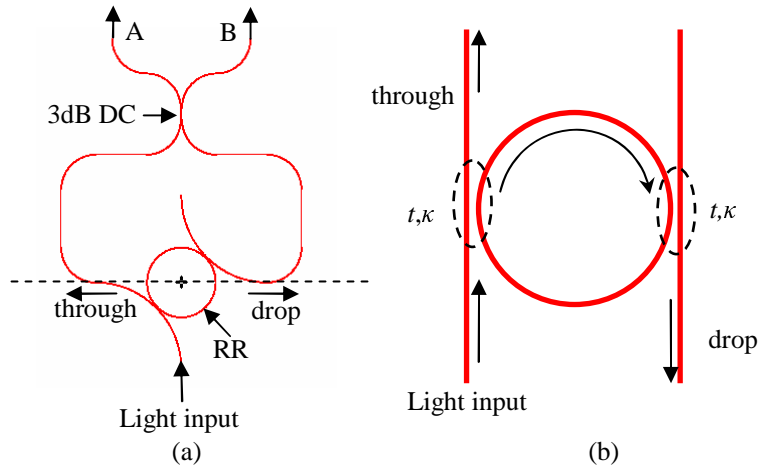


Fig. 1. (a) Schematic of the RR-MZI comprised of a RR that replaces the directional coupler of a conventional MZI and a 3 dB directional coupler in the RR-MZI output terminal. (b) RR structure.

A common MZI-based interleaver is comprised of two DCs or Y-branches in the input and output terminals and a delay line in one of the arms. The length of the delay line determines the free spectral range (FSR). We replace the input terminal with a ring resonator (RR) to form the proposed RR-MZI structure shown in Fig. 1(a). When light is launched into the bottom waveguide, it will be coupled into the RR and then split into through lights and drop lights. Finally, the lights will be recombined at the output through the 3 dB DC. The RR structure shown in Fig. 1(b) is comprised of a ring and two bus waveguides. In the following discussion we assume that the self-coupling coefficient (t) and cross-coupling coefficient (κ) are constant in the two coupled points of the RR, and $t^2 + \kappa^2 = 1$. The transmission functions of the through and drop channels are described in Eq. (1):

$$\begin{cases} H^{(through)} = \frac{E^{(through)}}{E^{(input)}} = \frac{t[\gamma \exp(i\theta) - 1]}{t^2 \gamma \exp(i\theta) - 1} \\ H^{(drop)} = \frac{E^{(drop)}}{E^{(input)}} = \frac{\sqrt{\gamma} \exp(i\theta/2) \kappa^2}{t^2 \gamma \exp(i\theta) - 1} \end{cases}, \quad (1)$$

where, H denotes the transfer function, which is a ratio between the input and the output wave functions. θ is the total phase shift for light that runs one round in the ring and can be described as: $\theta = n_r L_c k_0 = n_r L_c \omega / c$. Since θ is a function of frequency ω , we will not distinguish θ and ω in the following discussion. L_c is the circumference of the ring, k_0 is the wave number of the vacuum, and c is light velocity in the vacuum. We define the amplitude loss coefficient as $\gamma = \exp(-n_i L_c k_0)$. Where n_r and n_i are the real and imaginary parts of the effective refractive index, respectively.

As light will be delayed owing to the oscillations in the ring, the phase shift is step-like. Figure 2(a) shows the plot of the phases of the through and drop lights as a function of the light frequency. The blue and red curves denote the through and drop lights, respectively. The phase shifts are periodic functions of light frequency, and the period of the frequency of the drop light is two times of that of the through light. It can be easily understood from Eq. (1) that the through light will propagate full rounds in the ring before coupling out, while the drop light will run an additional half round. This half round becomes a delay line. It should be

noted that in Fig. 2(a), in the abscissa regions of (-4~ -2) and (0~ 2), the phase of the through light is $\pi/2$ greater than that of the drop light, whereas in (-2~ 0) and (2~ 4), the phase of the through light is $\pi/2$ smaller than that of the drop light. The directional coupler also provides an additional phase delay of $\pi/2$, shown in Eq. (2) between the straight and cross lights in leads A and B. Figure 2(b) shows the phase differences between the through and drop lights in leads A and B. Both the phase shifts increase to π alternately, demonstrating alternating light construction and destruction in the leads. The phase shifts of leads A and B shown in Fig. 3 are expressed also in Eq. (2)

$$\begin{cases} |H^{(A)}|^2 = \frac{1}{2} |H^{(through)} + iH^{(drop)}|^2 = \frac{X(\theta)^2}{X(\theta)^2 + Y(\theta)^2} \\ |H^{(B)}|^2 = \frac{1}{2} |iH^{(through)} + H^{(drop)}|^2 = \frac{Y(\theta)^2}{X(\theta)^2 + Y(\theta)^2} \end{cases}, \quad (2)$$

where

$$\begin{cases} X(\theta) = \kappa^2 + 2t \sin(\theta) \\ Y(\theta) = \kappa^2 - 2t \sin(\theta) \end{cases}.$$

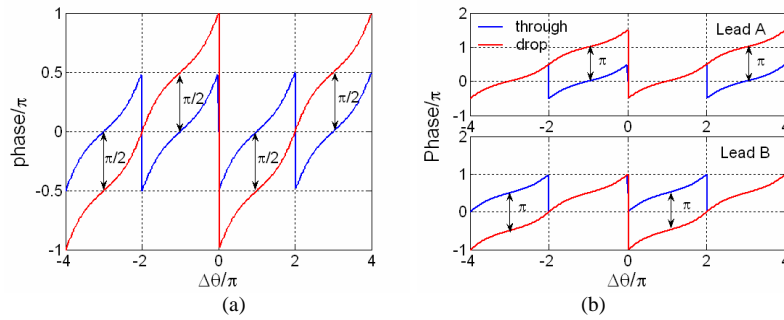


Fig. 2. (a) Phase shifts of the through and drop lights after RR. The phase difference between the through (blue curve) and drop (red curve) lights as a function of $\Delta\theta$ (frequency) is $+\pi/2$, $-\pi/2$, alternately. Fig. 2(b) shows the phase shifts of the through and drop in the lead A and B, respectively. Phase difference between them is 0, π alternately.

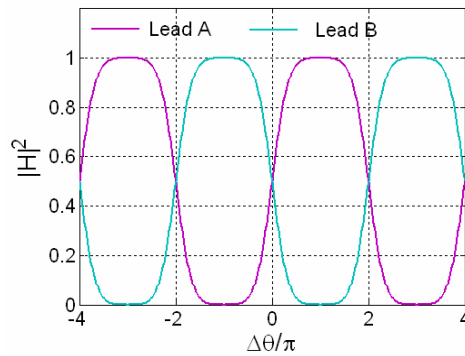


Fig. 3. Relative light intensities of leads A and B versus frequency.

2.2 Design optimization

The intensity of the output light is determined by the degree of coupling between the waveguide and the ring. For an idealized lossless situation ($n_i=0$), Fig. 4 shows how $|H|^2$ (relative output light intensity) varies with the self-coupling coefficient t . If t is in the region of (0.23 0.63), $|H|^2$ is larger than -0.5 dB, and if in the region of (0.33 0.51), $|H|^2$ is larger than -0.1 dB. However, in Fig. 4(b) when t is near 0 or 1, the intensities in the two leads are equal. At these two points, the device fails to function as an interleaver. For the outputs of a 3 dB coupler, the best situation is that the amplitude in the through channel is equal to that in the drop channel. Thus, we can easily obtain $t = \sqrt{2} - 1$. Interestingly, $|H|^2$ is flat in the peak, as shown in Fig. 3. Consequently, we can obtain Eq. (3) from Eq. (2). In lead A the flat-tops are at $\sim (4N+1)\pi$, while in lead B the flat-tops are at $\sim (4N-1)\pi$. In this situation, the device functions just as a 2nd-order Butterworth filter with maximum flat-top modality.

$$\begin{cases} |H^{(A)}|^2 = \frac{1}{1 + \tan^4\left(\frac{\pi - \theta}{4}\right)} \cong \frac{1}{1 + \left(\frac{\pi - \theta}{4}\right)^4} & \text{when } \theta \rightarrow (4N+1)\pi \\ |H^{(B)}|^2 = \frac{1}{1 + \tan^4\left(\frac{\pi + \theta}{4}\right)} \cong \frac{1}{1 + \left(\frac{\pi + \theta}{4}\right)^4} & \text{when } \theta \rightarrow (4N-1)\pi \end{cases} \quad (3)$$

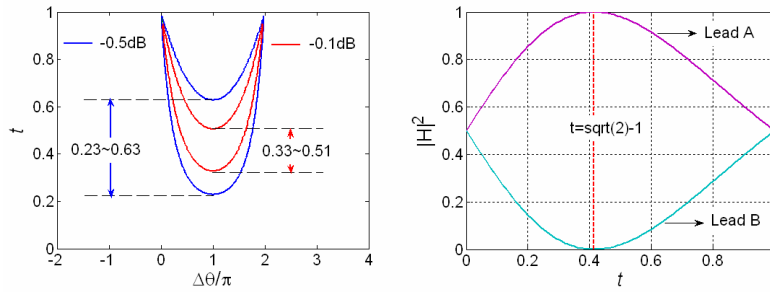


Fig. 4. (a) Transmission of Lead A; if t is in the region of 0.23~0.63, the relative light intensity loss is less than -0.5 dB; if in the region of 0.33~0.51, the loss is less than -0.1 dB. (b) $|H|^2$ is varied with the self-coefficient under the condition of lossless, *i.e.*, $\Delta\theta=\pi$. $t = \sqrt{2} - 1$ is denoted by red dashed line.

Finally, for the best situation where $t = \sqrt{2} - 1$ and $\gamma=1$, we can plot the passband, the rejection band, the phase shift, and the group delay response as shown in Fig. 5. The FSR, the -1 dB passband width, the -3 dB bandwidth, the -20 dB rejection bandwidth, and the -25 dB rejection bandwidth are $\Delta\theta=4\pi$, ~ 0.4 FSR, ~ 0.5 FSR, ~ 0.20 FSR, and ~ 0.15 FSR, respectively. The phase shift of the passband is shown as a red curve in Fig. 5(c). The red curve is roughly linear. The group delay time is defined as

$$\tau = -\frac{\partial\phi}{\partial\omega} = -T_c \frac{\partial\phi}{\partial\theta}, \quad (4)$$

where T_c is the time of light running a full round in a ring, and the group delay time is dependent on T_c . Thus we have equation:

$$\frac{\partial\phi}{\partial\theta} = \frac{\sqrt{2}}{3 - \cos(\theta)}. \quad (5)$$

The equation is plotted as a blue curve in Fig. 5(c), where the maximum and minimum are 0.707 and 0.354, respectively. If the interleaver is working as converter between a DWDM and a WDM system, FSR=100 GHz and $T_c=20$ ps, the group delay time is -7 ps ~ -14 ps. Since our structure is a one-stage filter, the group delay time will be shorter than those of multistage filters.

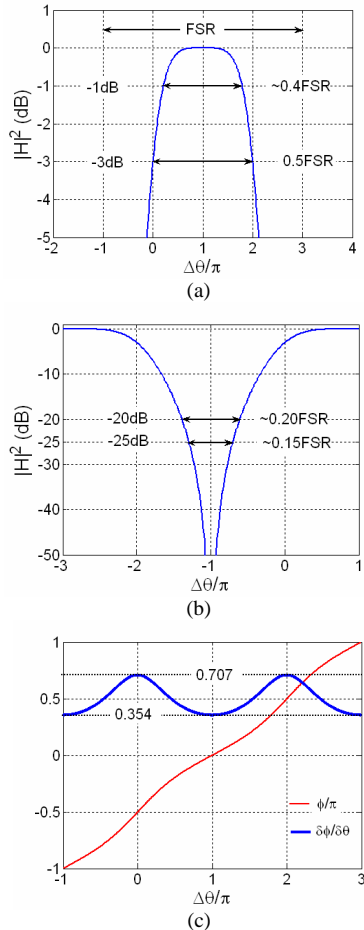


Fig. 5. (a) Characteristics of the passband. (b) Characteristics of the rejection band. (c) Characteristics of the phase and the relative group delay of the proposed interleaver.

3. Fabrication and characterization

3.1 Fabrication

We started the fabrication on a commercial 200 mm silicon-on-insulator (SOI) wafer with standard complementary metal-oxide semiconductor (CMOS) technology. Thicknesses of the top silicon layer and the buried silicon dioxide layer are 400 nm and 2 μm , respectively. First we oxidized and thinned the top silicon layer to 300 nm and then used 248 nm deep UV lithography to pattern the wafer. It is worth mentioning that we obtained the optimized pattern with focus-exposure modeling (FEM) in the lithography. We used the inductively coupled plasma etching system to etch down the top silicon layer. Then we cleaned the wafer with diluted HF and a sulfuric acid–hydrogen peroxide mixture. Moreover, to decrease the waveguide surface roughness, we thermally oxidized 5 nm-thick silicon for the etched silicon patterns [19]. Finally we deposited 3 μm -thick silicon dioxide on the wafer with plasma-

enhanced chemical-vapor deposition. The SEM picture of the main structure is shown in Fig. 6(a). Different from that shown in Fig. 1(a), the ring in Fig. 6(a) is replaced with a racetrack. The replacement is just for convenience of design. The cross-section of the silicon wire was chosen as $\sim 300 \times 300$ nm, as a waveguide with near square cross-section has less birefringence. Otherwise, the propagating TE and TM modes with different transmission constants will oscillate at different wavelengths, causing channel crosstalk and deterioration of the transmission spectrum. Figure 6(b) shows a fabricated 3 dB DC. Based on [20], we chose the coupling length as only 2.79 μm . A shorter coupling length will make the transmission spectrum flatter. The racetrack structure is shown in Fig. 6(c), where the radius of the silicon wire bend is 10 μm . The coupling length between the ring and the waveguide is 4.7 μm , and the radii of the two arcs connecting the two couplers are 4.191 μm . The circumference of the racetrack can be calculated as ~ 54 μm . Figure 6(d) is the SEM picture of the cross-section of the 3 dB DC. The coupling gap between the coupling waveguides is ~ 300 nm.

We have added spot-size converters (SSC) to the waveguides to increase the fiber-waveguide coupling efficiency, because the effective index and mode field of a SSC would match with those of a fiber. The SSCs are tapered waveguides and are widely used for coupling light between a submicron waveguide and a fiber [21, 22]. The tip width and length of the taper are 150 nm and 200 μm , respectively, as shown in Fig. 6(e). The full length of the interleaver device is 3 mm. Before measurement, we polished the input and output facets of the diced samples. The roughness in the polished facets is ~ 100 nm.

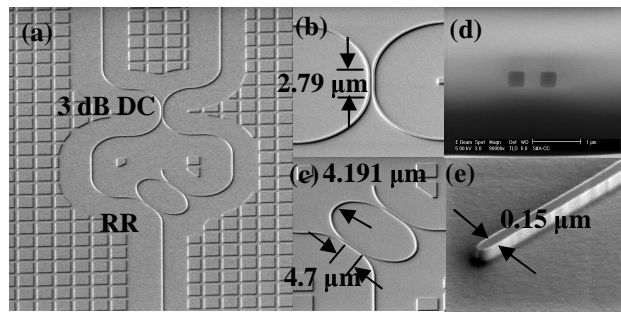


Fig. 6. (a) SEM picture of the RR-MZI. (b) 3 dB directional coupler; the coupling length is 2.79 μm and the coupling gap between two waveguides is 300 nm. (c) Coupler with the incident waveguide and the ring resonator; the coupling length is 4.7 μm and the contact arc radius is 4.19 μm . (d) SEM picture of a cross section of the DC; the gap between the two waveguides is ~ 300 nm. (e) SEM picture of SSC; the width of the tip is 150 nm and the length of taper is 200 μm .

3.2 Measurement results and analyses.

In the following measurement results, the insertion loss (IL) was recorded as the fiber to fiber loss, which included the device transmission loss and the coupling losses between a fiber and a SSC. Two lensed polarization-maintaining fibers (LPMF) were coupled with the input and output silicon wires, respectively. The focus spot size of the LPMF was ~ 2.5 μm . We scanned the wavelength from 1510 to 1580 nm with steps of 5 pm (EXFO IQS-12004B). The average insertion losses and the polarization dependent losses (PDL) of leads A and B are shown in Figs. 7 (a) and 7(b), respectively. PDL is commonly defined as the peak-to-peak difference in transmission for light with various states of polarization. We can observe that the tops of the spectra responses are flat. In the passband, the FSR, the IL, and the PDL are ~ 20 nm, ~ 10 dB, and < 5 dB, respectively; in the rejection band, the IL is ~ 20 dB, which means that the crosstalk is only ~ 10 dB. Although the PDL is a little bit high, it is not important for the rejection band.

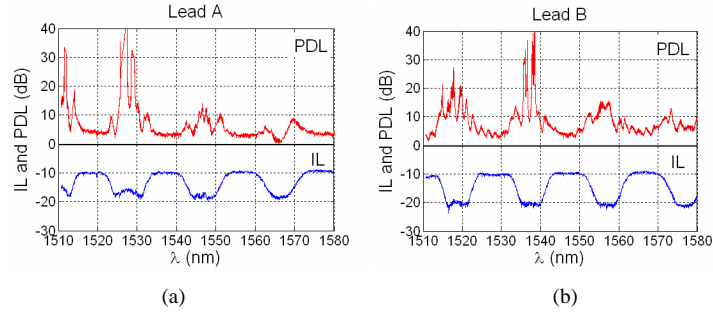


Fig. 7. (a) IL and PDL of lead A. (b) IL and PDL of lead B.

To understand the loss further, we measured the PDLs of both the silicon wire waveguides and the DCs. First we used the cut-back method to measure the PDL. We used eight waveguides with different lengths. The lengths of the waveguides increased from 3.4 mm to 7.6 mm with incremental steps of 600 μm . We measured four polarization states: parallel, diagonal, vertical, and circular for every waveguide. Then we obtained the IL of unit length waveguides for those four polarization states. Using the Mueller–Stokes analysis, we deduced the maximum and minimum ILs. To calculate the PDL of the SSC, we needed to subtract both the propagation loss of the straight waveguide and the bend loss of the four 180° bends of radius 5 μm . We also built 202 90° bends in a waveguide. Based on the IL difference between the bending waveguide and the straight waveguides, we calculated the bend loss of a 90° bend. The scanning wavelength was also varied from 1510 to 1580 nm with steps of 5 pm. The maximum and minimum ILs are shown in Fig. 8(a). The minimum loss is between 0.5 to 0.6 dB/mm and the maximum loss is between 1.0~1.2 dB/mm. Both the loss curves fluctuate with the wavelength. The PDL for the waveguide is 0.2~0.6 dB. Figure 8(b) presents the minimum and maximum losses of the SSC, which show opposite trends in the scanned wavelength range due to mode conversion in the tapered waveguide.

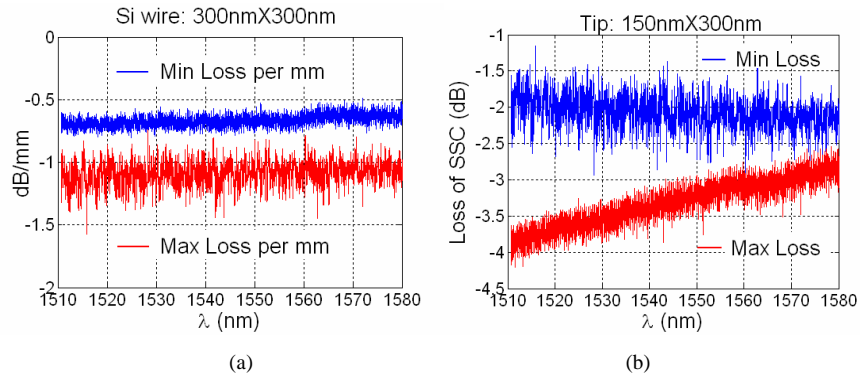


Fig. 8. (a) Measured losses of silicon wire. (b) Measured losses of SSC.

We also measured losses of the 3 dB DC and the RR DC. The results are presented in Figs. 9(a) and 9(b), respectively. Every DC we measured was a single device. The full length of the DCs with two SSCs is 3 mm. The middle parts of the DCs are shown in Fig. 6(b). Figure 10(a) presents the result of a 3 dB DC. For the output terminals of a straight and a cross waveguide of the DC, the PDLs are ~ 5 dB and < 5 dB, respectively. For the RR DC, the PDL of the straight waveguide is greater than 7 dB, and the PDL of the cross waveguide is less than 5 dB. Furthermore, the power in the straight waveguide is greater than that in the cross waveguide. For easy comparison with the straight waveguide, we put a reference IL in Fig. 9 (purple curve). The loss difference between the two DCs (black curve and purple curve) is ~ -2.0 dB. Note that the DC structure we measured included four 90° arcs with a radius of 10 μm . The

loss difference is also caused by the roughness near the coupling region of two waveguides in the RR DC.

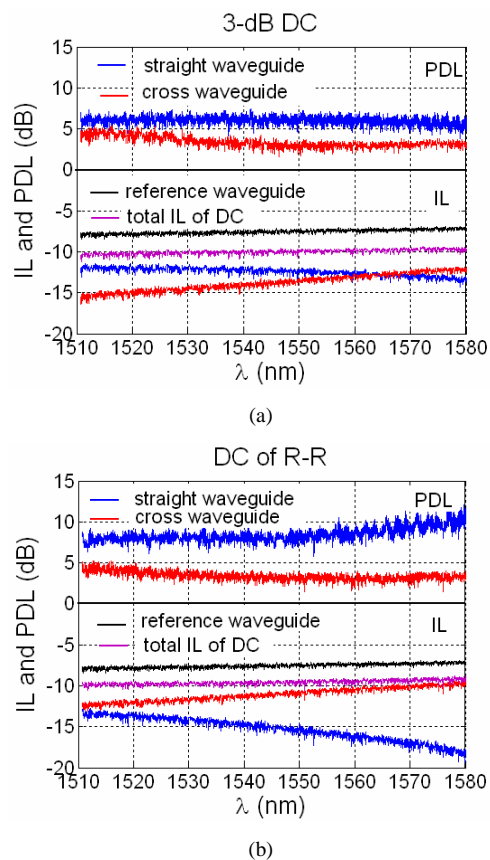


Fig. 9. (a) Measured losses of the 3 dB DC. (b) Measured losses of the DC of the RR; the blue and red curves denote straight and cross waveguides, and the black curve represents the reference waveguide. Both DCs have the same full length. The purple curve represents the total insertion loss of DC.

Since the coupling loss is large, we have to revise Eq. (2). Considering the loss and phase shift of the DC, we obtain the final related output intensity as Eq. (6)

$$\begin{cases} |H^{(A)}|^2 = \frac{[X(\tilde{\theta}) - \Delta p^2 t \sin(\tilde{\theta})]^2 + [\Delta p^2 t \cos(\tilde{\theta})]^2}{[\Delta p^2 + X(\tilde{\theta})]^2 + [\Delta p^2 + Y(\tilde{\theta})]^2} \\ |H^{(B)}|^2 = \frac{[Y(\tilde{\theta}) + \Delta p^2 t \sin(\tilde{\theta})]^2 + [\Delta p^2 t \cos(\tilde{\theta})]^2}{[\Delta p^2 + X(\tilde{\theta})]^2 + [\Delta p^2 + Y(\tilde{\theta})]^2} \end{cases}, \quad (6)$$

where $\tilde{\theta} = \theta/2 - \theta_t$, $p^2 = t^2 + \kappa^2$, and $\Delta p^2 = 1 - p^2$. θ_t is the additional phase shift. When $\Delta p^2 = 0$ and $\theta_t = 0$, the equation returns to the ideal situation. The loss of the DC of the RR influences the crosstalk, evidently. Figure 10 shows the effect. When p^2 decreases, t decreases, too.

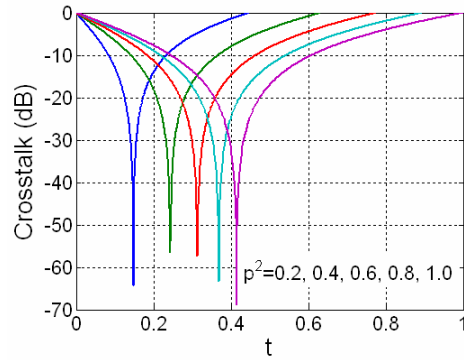


Fig. 10. Crosstalk versus loss in the RR DC. p^2 is reduced from 1.0 to 0.2 by steps of 0.2, and the corresponding curves are arranged from right to left.

Considering Fig. 9, we estimate that $p^2 = 0.62$, and the angle of the 3 dB DC is 41.4° . Moreover, we estimate $\gamma = 0.95$, the group refractive index $n_g = 4.5$, and $\theta_t = 0.85\pi$. The measurement and the fitting curves are shown in Fig. 11. Both the results are compatible despite the ignored dispersion relation of the DC.

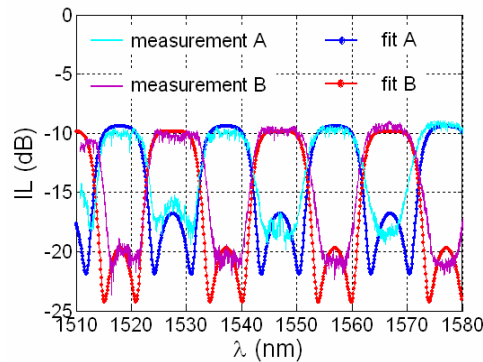


Fig. 11. Measurement and fitting results.

From the above discussion, we can conclude that the 3 dB DC influences the symmetry of leads A and B, and the RR DC influences the crosstalk, which includes the self-coupling coefficient t and the loss p^2 . To control the splitting ratio of a DC in future design, we can use the thermal-optical method as in [16-18]. Generally, the loss in a MMI is less than that of a DC. Therefore, we can replace the DCs with MMIs. For example, a MMI with a splitting ratio

of 15:85 can be used to replace the RR DC, and a 2×2 MMI with a splitting ratio of 50:50 can be used to replace the 3 dB DC.

4. Conclusion

We have demonstrated a novel RR-MZI interleaver structure, which is comprised only of a ring and a 3 dB DC. The proposed interleaver is more compact and easier to design. Theoretically, the -1.0 dB and the -3.0 dB pass bandwidths can be as wide as ~ 0.4 FSR and ~ 0.5 FSR, respectively. The -20 dB rejection bandwidth is ~ 0.20 FSR, and the -25 dB bandwidth is ~ 0.15 FSR. We have experimentally characterized the performances of this interleaver structure based on $300 \text{ nm} \times 300 \text{ nm}$ silicon wires. The interleaver has a flat-top spectral response. The measured PDL is < 5 dB, and the IL is ~ 10 dB. This interleaver structure can be constructed not only on high-index contrast materials but also on low-index contrast materials such as silica, fiber, silicon nitride, and so on.